Observation of the bulk ion density peaking in a discharge with an impurity hole in the LHD

Observation of the bulk ion density peaking in a discharge with an impurity hole in the LHD

A Perek[1], K Ida[2], M Yoshinuma [2], M Goto[2], Y Nakamura[2], M. Emoto[2] and LHD Experiment Group[2]

[1] Eindhoven University of Technology, 5612 AZ Eindhoven, The Netherlands
[2] National Institute for Fusion Science, Toki, Gifu, 509-5292, Japan

E-mail: ida@nifs.ac.jp

Abstract. Radial profiles of bulk ion and impurity ions density are simultaneously measured and quantified using charge exchange spectroscopy and peaking parameter, C_{v}. The peaking parameter is positive for inward and negative for outward convection in a plasma with an impurity hole in the Large Helical Device. Following the formation of an impurity hole associated with the transition from L-mode to ion ITB plasma, the bulk ion becomes peaked by the inward convection ($C_{\mathrm{v}} > 0$), while impurities (helium and carbon) become hollow due to the outward convection ($C_{\mathrm{v}} < 0$). In contrast to the ion ITB plasma, in the L-mode plasma the impurity profiles are peaked ($C_{\mathrm{v}} > 0$), where the bulk ion density profile remains flat ($C_{\mathrm{v}} \sim 0$). Understanding of the impurity behavior in the ion ITB plasma could lead to a self cleaning plasma reactor concept, with an efficient impurity exhaust.

PACS numbers: 52.55.Hc 52.25.Fi 52.50.Gj

Submitted to: *Nucl. Fusion*

1. Introduction

Improved plasma confinement of a nuclear fusion reactor leads to a better performance of the device. However, the confinement of impurities can also decrease the performance. Impurities dilute the plasma and increase radiation depending on the Z number. The desired confinement characteristics would be an efficient exhaust of impurities combined with an improved confinement of hydrogen. The desired confinement characteristics were observed in HDH discharge in Wendelstein 7AS and impurity hole discharge in LHD [1–3]. The impurity transport can be determined by several processes: collisions between bulk ion and impurities [4], radial flux due to the electric field and turbulence driven flux [5–7]. The momentum exchange between bulk and impurity ions results in an inward impurity flux by the bulk ion density gradients and an outward impurity flux driven by bulk ion temperature gradients (gradient of collision frequency), which is called the temperature screening. In tokamaks, the temperature screening depends on the collisionality regimes of the plasma species and it does not occur universally [8]. The effect has not been proven for stellarators. Therefore peaked impurity profile is expected in a peaked density and flat temperature profile plasma, while hollow impurity profile is expected in the peaked temperature and flat density profile plasma. Radial fluxes in the opposite direction between bulk ion and impurity (inward impurity flux and outward bulk ion flux and vice versa) are the phenomena directly predicted by the basic process of momentum exchange between bulk ion and impurity. However, the radial fluxes in the opposite direction between bulk ion and impurity have not been yet observed in an experiment due to lack of the bulk ion density profile measurements.

Recently at the LHD a two-wavelength spectrometer was installed to measure radial density profiles of hydrogen and helium employing HI and HeII charge exchange lines. Simultaneous measurement of both hydrogen and helium also provides the radial profile of helium to hydrogen density ratio [9]. The two-wavelength spectrometer is a powerful tool to study transport of helium, the ash of the nuclear fusion reactions which is an active area of research focused on understanding and applying the helium transport to create a suitable helium exhaust [10–12]. Recent study of helium transport employing the two-wavelength spectrometer demonstrated a clear difference between helium and hydrogen transport in a low confinement (L-mode) discharge [13]. Contrary to an L-mode discharge, the nature of differences in transport of hydrogen and impurities in an ion ITB plasma discharge has not yet been studied sufficiently. The impurity hole is an extremely hollow density profile of impurities obtained in an ion ITB plasma and it was linked to a critical value of normalized ion temperature gradient [14, 15]. The phenomenon led to a measurement of radial electric field with use of a heavy ion beam probe revealing the negative sign of the field. According to the neoclassical theory, the negative sign of the field should lead to impurity accumulation in a nonaxisymmetric system. Therefore, the experiment contradicts the prediction of the neoclassical theory [16]. This fundamental difference in impurity behavior between the LHD and a tokamak where the ITB causes an inward convection of impurities led to a comparison of the dynamics of internal transport barriers between LHD and JT-60U [17]. In this paper, profiles of helium, hydrogen and carbon densities are measured with use of the charge exchange spectroscopy employing beam modulation technique with a frequency of 5 Hz to subtract the emission from plasma periphery [9, 18]. The electron density profile is measured with use of the Thomson scattering [19]. The density profiles of an ion ITB discharge are compared with L-mode discharge profile. The differences are presented by comparing the profiles over a broad range of the helium puff strength.

2. Peaking factor

The nature of an ion ITB plasma results in a relatively large change in carbon density gradient over the discharge. In an ion ITB shot, the usual carbon density prior to the pellet injection is in the following range $1 - 2 \cdot 10^{17}\,\mathrm{m}^{-3}$. After the injection, the density increases by an order of magnitude to the range of $1 - 2 \cdot 10^{18}\,\mathrm{m}^{-3}$, while the electron density is in the range $1 - 2 \cdot 10^{19}\,\mathrm{m}^{-3}$. The change in the carbon density enables the dynamic transport analysis which yields radial profiles of both the diffusion coefficient D and the convection velocity V. Positive V indicates outward convection where negative V indicates inward convection. The analysis employs the fact that the particle transport has a significant contribution to the transport by off-diagonal terms in the transport matrix [20]. What is more the radial flux of impurities

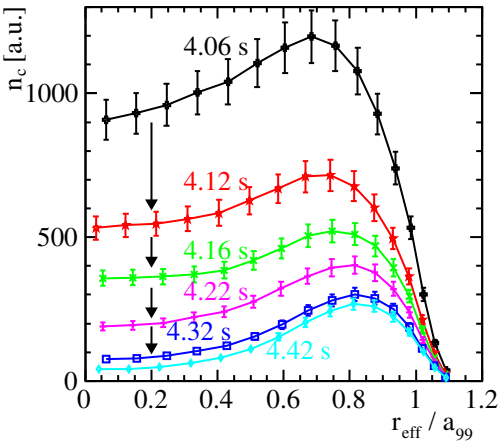

Figure 1. Time slices of the carbon density profiles with corresponding errors. Shot #97030.

normalized to the impurity density can be expressed as a sum of diffusive and non-diffusive terms which are diagonal and off-diagonal terms of the transport matrix respectively. Therefore the normalized radial particle flux can be written as:

$$\frac{\Gamma}{n_I} = -D\frac{\nabla n_I}{n_I} + V, \tag{1}$$

where the radial particle flux Γ and the density gradient ∇n are calculated form the time slices of the density profiles. The time slices of the carbon density profiles are presented in the figure 1. The original profiles were slightly scattered due to different transmission coefficients of the optical fibers on the level of a few percent. The scattering highly influenced the flux gradient relations creating not physical artefacts. Therefore, to avoid scattering, a number of profiles in proceeding and following discharges were fitted with an exponential function to find a series of correction factors, one for each fibre. The correction factors were applied for the discharge 97030, successfully removing unphysical artefacts from the flux gradient relations. The profile in 97030 was also fitted. However, due to the profile after the pellet ablation it was not the most successful fit of the entire profile. Therefore, it was fitted in two parts $r_{\rm eff}/a_{99} < 0.7$ and $r_{\rm eff}/a_{99} > 0.7$. The fit gave a very similar correction factors to the neighbouring shots. The root mean square value of the calibration factors was used to evaluate the error of the profile measurement. The radial particle flux at a given radius r can be expressed as:

$$\Gamma_I(r) = \frac{1}{r}\int_0^r r'\left[S(r') - \frac{{\rm d}n_I(r')}{{\rm d}t}\right]{\rm d}r'. \tag{2}$$

In this experiment the dynamic transport of carbon is evaluated, therefore the source term S can be neglected since there are no sources of carbon in the main plasma where $r_{\rm eff}/a_{99} < 0.9$. The only source of carbon is localized near the plasma edge, thus the points at the plasma edge will be neglected in the calculation. Under the assumption that the diffusion coefficient and convection velocities are constant in time during the analysis the relation between normalized flux and normalized gradient should follow a straight line. Linear fit of points obtained for each radial position provides the diffusion coefficient D in form of its slope and the convection velocity V as the intercept. As a result, the analysis yields radial profiles of both D and V. Provided both the diffusion coefficient and the convection velocity, one can calculate the radial profile of the peaking factor:

$$C_{\rm v} = -a^2V/(2Dr) \tag{3}$$

Figure 2 presents the results of the dynamic transport analysis of carbon performed on the shot number 97030 in the LHD. The NBI input power in the shot was 19 MW, the central values of the plasma parameters were: $T_{i0} = 5\,{\rm keV}$, $T_{e0} = 3.5\,{\rm keV}$, $n_0 = 1 - 2\cdot 10^{19}\,{\rm m}^{-3}$.

The particle flux Γ_I and the density gradient ∇n_I were evaluated from the carbon density profile evolution in the decay phase of the discharge after the ion ITB formation. The time evolution of the profile indicates that during the impurity hole discharge in the decay phase the density profile of carbon evolves until a certain hollow shape is obtained followed by a further decrease of the carbon density which can also be observed in the flux gradient relation in form of the range of change of the normalized density gradient. Figure 2a presents the relation between the normalized radial carbon flux and the normalized carbon density gradient obtained from the time slices at $4.24\,{\rm s}\pm 0.18\,{\rm s}$. The relation presents a linear dependence between normalized particle flux and the normalized density gradient confirming the validity of the assumption that the diffusion coefficient and the convection velocity are constant during the time interval of the analysis. Radial profile of the diffusion coefficient is presented in figure 2b with the corresponding error evaluated in the fitting procedure. The diffusion coefficient has a value of about $0.25\,{\rm m^2s^{-1}}$ in the center of the plasma and increases towards the edge where its value increases above $2\,{\rm m^2s^{-1}}$ past the point $r_{\rm eff}/a_{99} \approx 0.80$. The radial profile of the convection velocity is presented in figure 2c with the corresponding error evaluated in the fitting procedure. Evaluated convection velocity indicates positive, outward convection velocity in the main plasma $r_{\rm eff}/a_{99} < 0.85$ while in the plasma periphery $r_{\rm eff}/a_{99} > 0.85$ the convection velocity is negative, inward. Resulting combination of inward and outward convection velocity can in fact produce the

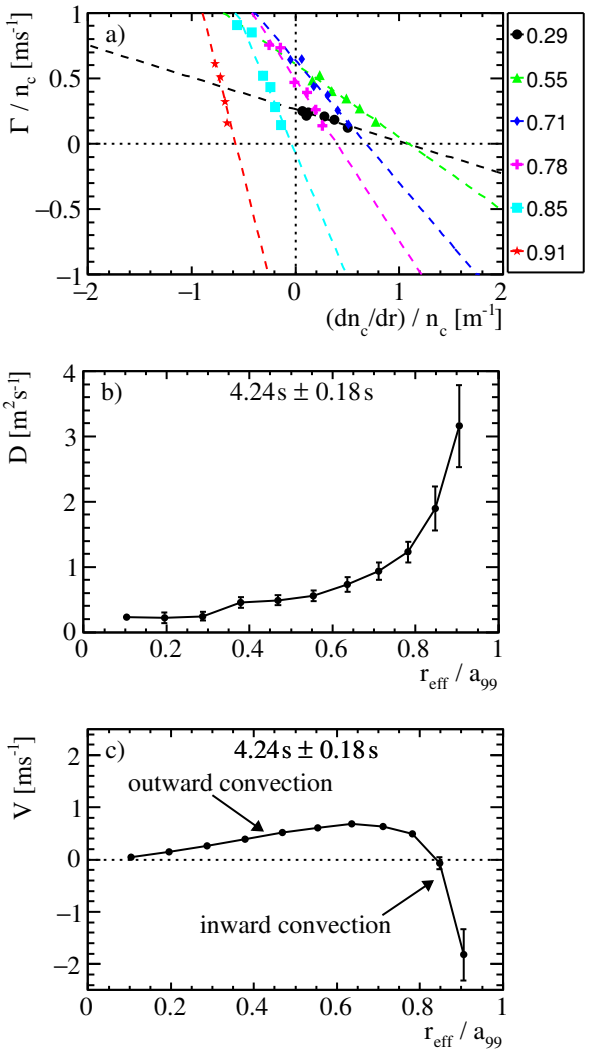

Figure 2. (2a) Normalized radial flux of carbon as a function of normalized carbon density gradient. (2b) Radial profile of the diffusion coefficient. (2c) Radial profile of the convection velocity.

hollow profiles peaked at $r_{\rm eff}/a_{99} \approx 0.85$, observed as the profiles reach steady state in figure 1.

The radial profiles of the diffusion coefficient and the convection velocity enable the calculation of radial profile of the peaking factor $C_{\rm v}$ with use of (3). The radial profile of the peaking factor presented in figure 3 shows a slight increase with an average value of about –1. As the value of the peaking factor increases with the normalized radius, it reaches zero at $r_{\rm eff}/a_{99} \approx 0.85$ with a smooth transition from negative to positive value. The result demonstrates that the peaking factor is within a range from about –2 in the plasma core up to 0.5 at the plasma periphery.

The average value of the peaking factor can also be evaluated from the density profile once a

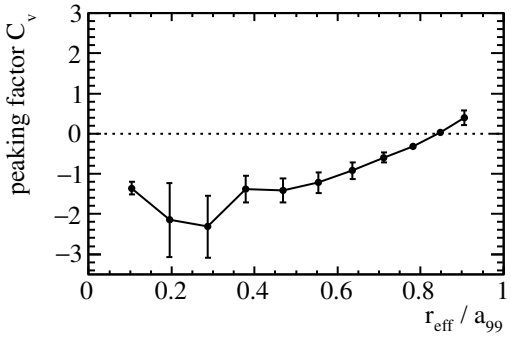

Figure 3. Radial profile of the peaking factor $C_{\rm v}$ averaged at 4.04 s – 4.42 s. The peaking factor was calculated from the radial profiles of the diffusion coefficient and the convection velocity with corresponding error bars.

steady state is reached in the later phase of the discharge when the impurity density profile becomes proportional to $\exp\left(-C_{\rm v}r^2/a^2\right)$ when the diffusion coefficient is constant in space and convection velocity is proportional to the plasma radius [21]. The steady state peaking factor can be evaluated from a ratio of impurity density at two different locations in the plasma. In this paper, the locations of the two points are: $\rho_1 = r_{\rm eff}/a_{99} \approx 0.5$ and $\rho_2 = r_{\rm eff}/a_{99} \approx 0.9$. Position of the inner point was derived from the diagnostic constrain to ensure reliable hydrogen and helium signals from the inner part of the plasma. The outer point was selected to place the location of the ITB in between those points [22, 23]. The steady state peaking factor can be expressed as:

$$C_{\rm v} = \frac{\ln\left(n_I(\rho_1)/n_I(\rho_2)\right)}{\rho_2^2 - \rho_1^2}. \qquad (4)$$

Positive peaking factor indicates that the profile is peaked, where the negative peaking factor is obtained if the profile is hollow while the near zero value indicates that the profile is flat. Consequently the peaking factor obtained from either analysis reflects the shape of the density profile and the sign of the convection velocity which can be exploited to quantify the time evolution of the profile. Interpreting the time slices of the profiles as quasi steady state profiles, one can evaluate a quasi steady state peaking factor $C_{\rm vqss}$. The time trace of the quasi steady state peaking factor will evolve as the profile evolves to reach a steady state defined by the ratio of the diffusion coefficient and the convection velocity, thus reaching the value of the steady state peaking factor $C_{\rm v}$. In this paper, the quasi steady state peaking factor $C_{\rm vqss}$ will be used to quantify the time evolutions of both the bulk ion and the impurity profiles. The value of the peaking factor $C_{\rm v}$ will be obtained as the value of the $C_{\rm vqss}$ when a steady state is reached in the last measured profile.

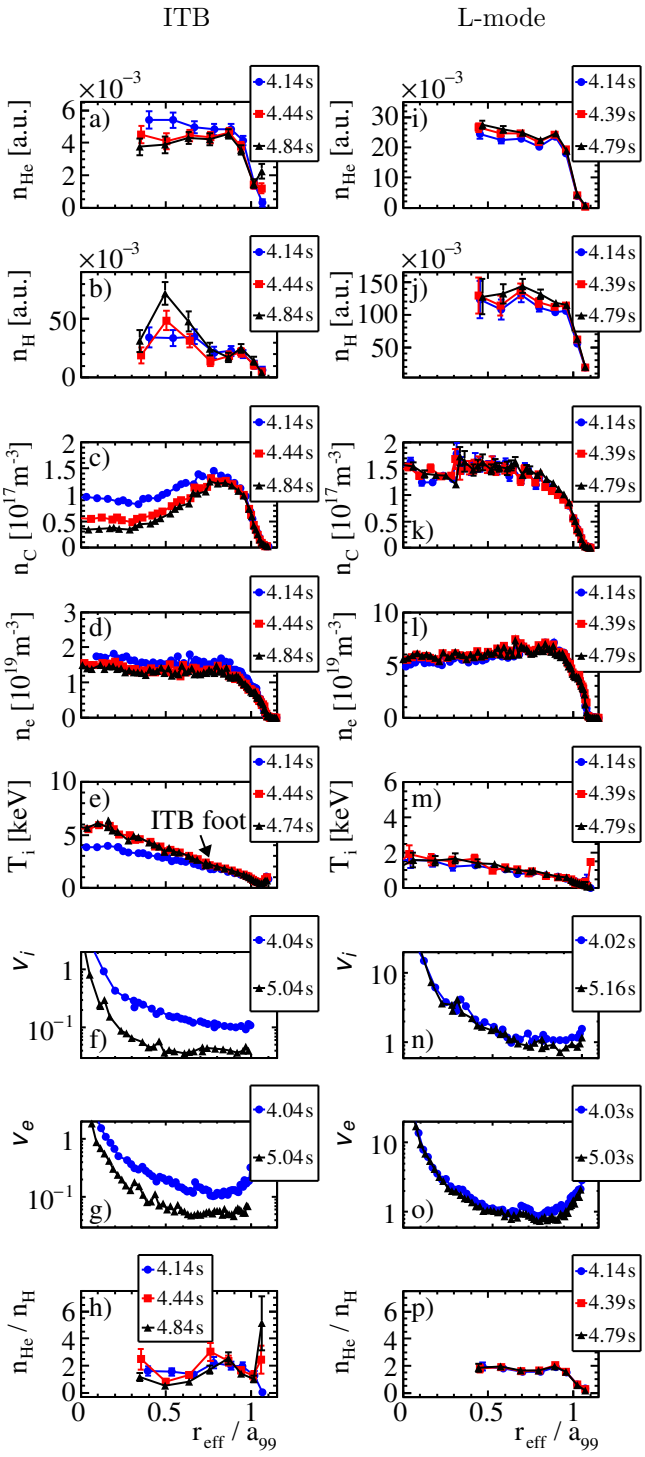

Figure 4. Radial profiles of (a)(i) helium, (b)(j) hydrogen, (c)(k) carbon, (d)(l) electron density, (e)(m) ion temperature, (f)(n) ion collisionality, (g)(o) electron collisionality and (h)(p) helium to hydrogen ratio in ion ITB plasma (a)-(h) and (i)-(p) in L-mode plasma.

3. Shot Comparison

Recent work presented the dependence in peaking of the bulk ion profile and impurity profile on the helium puff strength [13]. Therefore, for the purpose of this comparison the shots were selected with a similar helium puff strength, $n_{He}/n_H \sim 2$. The shot numbers are 128675 and 128037 for the ion ITB and L-mode discharges, respectively. The the main differences between the selected shots were the electron density and the NBI input power. The NBI input power was 25 MW for the ion ITB shot and 8 MW for the L-mode shot. Detailed description of the ion ITB scenario can be found in [22]. Figure 4 presents a comparison of the time evolution of the bulk ion and the impurity density profiles. In the ion ITB discharge the helium profile becomes slightly hollow where in the L-mode discharge the helium profile becomes slightly more peaked as the time advances indicating the impurity accumulation. The impurity accumulation in the L-mode is predicted by the neoclassical theory where the radial particle flux is driven by the radial electric field, such behavior was observed in long pulse discharge in the LHD [24, 25]. The L-mode impurity accumulation can be avoided by employing a discharge scenario with high density and low temperature in the scrape-off layer combined with generation of the magnetic islands at the plasma boundary and a certain degree of edge localized modes [26]. In these scenarios, the core impurity concentration is controlled by reducing the impurity influx in the scrape-off layer or by an enhancement of the edge outward convection. The ITB plasma discussed in this paper presents a control of core transport rather than the control of impurity flux or impurity transport in the scrape-off layer. Therefore, the enhancement of the outward convection is important from a perspective of the helium ash exhaust.

Due to the diagnostic constrains the most inner points of helium and hydrogen profiles are insensitive to fast changes of the intensity due to its integration time which can reach up to 1 s. What is more, the most inner points are also affected by the calculation of the beam attenuation which does not take into account halo effect nor cross section effect. Evaluation of the influence of both of those effects can be found in [9]. Therefore, those points are rejected in this analysis as inaccurate if a significant change of profile occurs. The helium density profile presented in figure 4a becomes hollow in the ion ITB discharge, where in the L-mode discharge it is slightly peaked in figurie 4i. The hydrogen profile visible in figure 4b becomes more peaked in the ion ITB discharge, where in the L-mode discharge the hydrogen profile presented in figure 4j remains flat with a slight density increase during the discharge. In the ion ITB discharge the location of the radial position within which the hydrogen density profile increases corresponds to the clearly visible location of the ion ITB foot in the ion temperature

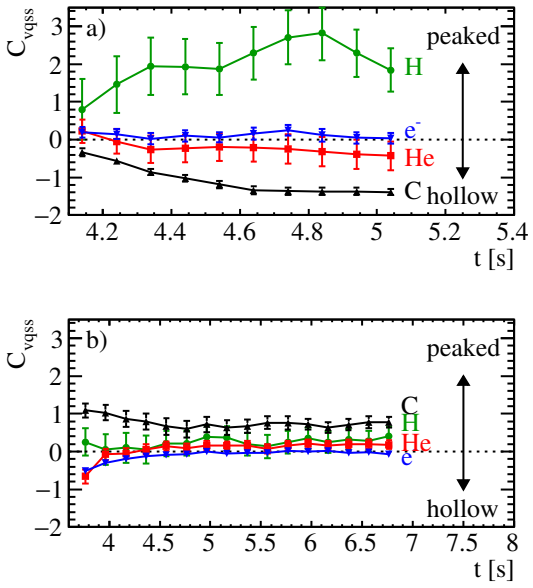

Figure 5. Time traces of the C_{vqss} for hydrogen, helium, carbon and electron density. (a) ITB discharge, (b) L-mode discharge.

profile presented in figure 4e. The location of the ion ITB also corresponds to the radial position at which carbon profile becomes hollow. The L-mode carbon profile shows that carbon is peaked in the center of the plasma. The carbon profiles are presented in figures 4c and 4k for the ion ITB and the L-mode, respectively. Both discharges show that the electron density profile in figures 4d and 4l is relatively flat and the profiles do not change during the discharge.

Figures 4f, 4g, 4n, 4o present the radial profiles of the ion and electron collisionalities for both cases. The collisionalities were evaluated as the collision frequency normalized to the particle bounce frequency of the banana orbit. The radial profiles of the collisionalities were calculated using the electron density, ion temperature and the magnetic field configuration with a finite-beta 3D equilibrium code VMEC. The ion ITB plasma presented in 4f and 4g, is in the collisionless regime with collisionality below 0.1 at $r_{\mathrm{eff}}/a_{99} \sim 0.5$. The regime is obtained by the combination of the high ion temperature with low electron density. On the other hand, in the L-mode case presented in 4n and 4o, the plasma is in the plateau regime where the collisionality at the $r_{\mathrm{eff}}/a_{99} \sim 0.5$ is close to unity. Thus, presenting a difference in collisionality regimes between the two discharges.

The analysis of the time evolution of the profiles can also be carried out with use of the concept of the quasi steady state peaking factor. Figure 5 shows the time evolution of the quasi steady state peaking factor in both discharges. In the ion ITB discharge the ITB develops with the start of the profile measurement and it decays at the end of the measurement where in the L-mode case there is no change of conditions during the measurement. The analysis shows a clear difference between hydrogen and impurity profiles in the ion ITB discharge. Observed hydrogen peaking is consistent with flat electron density profile and hollow impurity density profiles. Observed trends for hydrogen and the impurities indicate a coupling between the bulk ion and the impurity transport. As the time advances the impurities become more hollow and the hydrogen becomes more peaked while the rate of change decreases as the profiles achieve a steady state where the C_{vqss} becomes equivalent to the C_{v}. The time evolution of the quasi steady state peaking factor of the L-mode discharge does not illustrate a clear separation between the peaking factors of different plasma species. In fact all of the species are found in a narrow range of values of the peaking factor. The initially slightly hollow profiles of helium and electron density can be attributed to a helium puff. Comparison of the magnitudes of the peaking factor between the discharges indicates a clearly visible difference in transport.

4. Effect of helium puff strength on the bulk ion and impurity transport

A recent study presented a clear difference between hydrogen and helium transport in the LHD comparing the peaking factor C_{v} of hydrogen and helium for a number of L-mode discharges in a broad spectrum of helium puff [13]. The study found that as the helium fraction in the plasma increases, initially peaked helium profile becomes less peaked and even slightly hollow while the hydrogen from peaked profile becomes flat and peaked again. The change of the peaking factors indicates that the peaking of the helium density profile becomes more apparent when the helium fraction decreases and helium becomes impurity. For the purpose of comparison between the L-mode and the ion ITB plasma, the referenced study of the L-mode plasma was repeated and extended to include peaking factors of electron and carbon density profiles. In order to compare the ion ITB and the L-mode plasma, a set of conditions was imposed as selection rules to separate the discharge into an ion ITB with an impurity hole or an L-mode category. Previous studies of the impurity hole showed that the flow of impurities can be reversed during the impurity hole formation. Therefore, a steady NBI power input is required combined with the steady state of the carbon profile [27]. The NBI modulation used for the charge exchange spectroscopy was 80 ms ON and 20 ms OFF.

The shots are also required to achieve a steady state profile of impurities so that the quasi steady state peaking factor becomes a steady state peaking factor. The impurity hole should also be clearly visible in the steady state density profiles. To qualify a shot as an ion ITB, the ratio between central ion and electron temperature should be higher than 1.1, and in the case of an L-mode the ratio should be lower than 1.1. The magnetic configuration should be the same for all discharges. In this analysis, the position of the magnetic axis was $R_{\rm ax} = 3.6\,$m. The parameter ranges for the ion ITB case were as follows: $T_e = 3 - 3.5\,$keV, $Ti = 3.6 - 6\,$keV, $n_e = 1 - 2 \cdot 10^{19}\,$m^{-3}. The parameter space for the L-mode case was: $T_e = 1.3 - 3\,$keV, $Ti = 1.3 - 2.7\,$keV, $n_e = 2 - 5 \cdot 10^{19}\,$m^{-3}.

Figures 4h and 4p show the profiles of helium to hydrogen ratio. The profile of ratio becomes hollow in the ion ITB discharge where the value of the ratio outside the ion ITB is nearly unaffected by the transition from the L-mode to the ion ITB plasma. In the L-mode discharge the ratio remains flat over the discharge. The difference in transport between the L-mode and the ion ITB discharge results in a radial dependence of the helium to hydrogen ratio. The dependence of the ratio makes the definition of helium fraction in the plasma dubious. Therefore, in this paper, instead of quantifying the helium fraction in the plasma, the strength of helium puff will be used to quantify the amount of helium entering the plasma. In the LHD the strength of the helium puff, i.e., influx into the plasma, can be derived from the intensity ratio of H_α (656.3 nm) and HeI (667.8 nm) [28]. In previous works the influx was found to be directly proportional to the helium to hydrogen ratio at the $r_{\rm eff}/a_{99} \approx 0.9$ for the L-mode plasma [13]. Since the ratio at $r_{\rm eff}/a_{99} \approx 0.9$ is nearly unaffected by the transition from the L-mode to the ion ITB plasma it will be used to quantify the amount of helium puffed in both types of discharge. The ratio of about ~ 0.1 corresponds to a weak helium puff, where the ratio of ~ 3 is a strong helium puff. Unfortunately, in an ion ITB discharge a helium puff of ~ 0.2 can be provided by recycling alone, thus rendering shots with a very low helium puff unavailable.

Comparison of the peaking factor of the bulk ion and the impurities between the ion ITB and the L-mode discharges is presented in figure 6. In the ion ITB discharge set presented in (a)-(d) the hydrogen profile becomes clearly peaked, with the magnitude of the peaking factor varying from 0.2 (slightly peaked) up to 2 (strongly peaked). Helium profile becomes slightly hollow with the peaking factor between –0.1 (slightly hollow) to –1.5 (strongly hollow). The electron density profile remains flat and independent of the helium puff strength for the ITB case, where for the L-mode

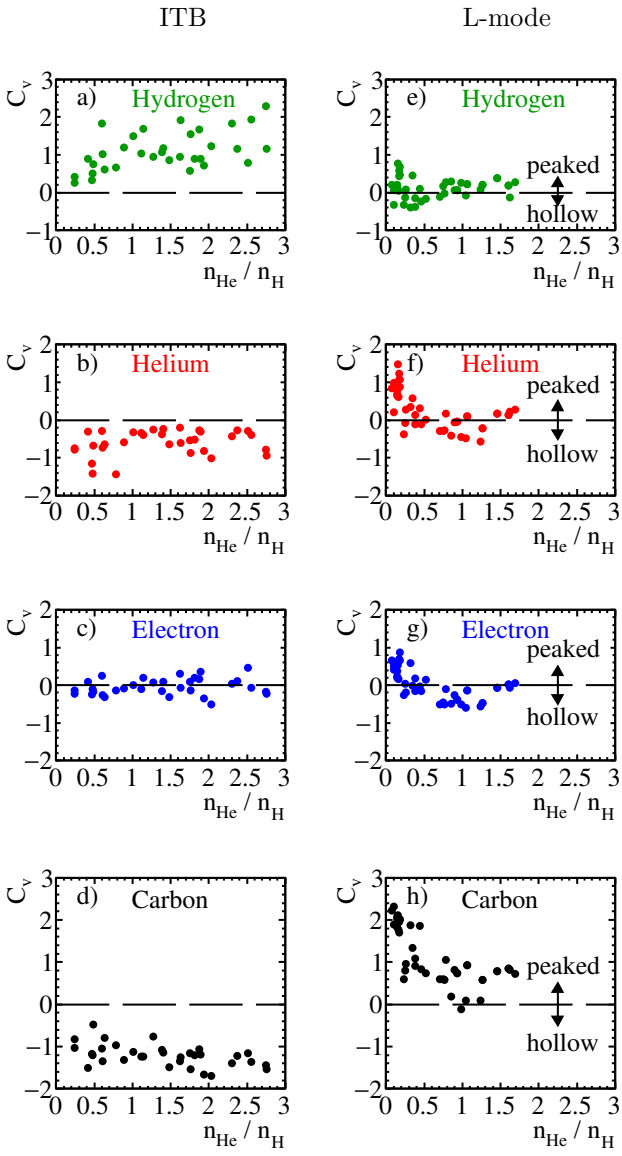

Figure 6. Peaking factor $C_{\rm v}$ of (a)(e) hydrogen, (b)(f) helium, (c)(g) electron, (d)(h) carbon density in the ITB plasma (a)-(d) and (e)-(h) in the L-mode plasma as a function of helium puff strength.

discharge the profile from peaked to hollow. Carbon density profile becomes hollow for all of the ITB discharges with the peaking factor varying from –0.2 (slightly hollow) down to almost –2 (strongly hollow). In the case of the L-mode the carbon from strongly peaked becomes less peaked as the plasma becomes helium dominant. In the ion ITB shots, the separation of the peaking factors of hydrogen as the bulk ion from the impurities clearly illustrates differences in transport during the ion ITB discharge. The ordering of the peaking factors of the impurities clearly follows the Z-dependence presented in the previous work [29].

In contrast to the ion ITB discharges, the L-mode

study presented in (e)-(h) does not indicate any clear separation between convection sign between different species. In the L-mode, as the helium fraction increases the peaking factors of helium and carbon significantly decrease from 1.5 and 2 to –0.4 and 0.5, respectively. Additionally, at the low helium fraction the peaking factor of helium and carbon becomes higher. The result suggests that there is a Z-dependence of the inward convection in the L-mode. The higher the Z number of an impurity, the larger the inward convection. This result suggests that the impurity accumulation could be a serious problem when the high Z impurities are present in a reactor.

5. Discussion and summary

Simultaneous evolution of hydrogen, helium, carbon, and electron density profiles was observed and quantified. The quantification of the profile evolution based on a quasi steady state transport analysis indicates a very clear difference in transport between the ion ITB and the L-mode discharges. An interesting impurity behavior was observed in the ion ITB plasma, where the bulk ion becomes peaked as the impurity density profiles become hollow. Such effect was not observed in the L-mode case.

Dependence of the peaking factor on the strength of the helium puff was presented with a steady state analysis. The steady state analysis was supplemented by the dynamic transport analysis deriving the radial profile of the peaking factor $C_{\rm v}$ which was found to range from about –2 in the plasma core up to 0.5 at the plasma periphery for carbon. The peaking factor obtained in the dynamic analysis of carbon impurity $C_{\rm v} \sim 0.5$ at $r_{\rm eff}/a_{99} = 0.75$ was found within factor 2 from the $C_{\rm vqss} \sim -1$ found in the steady state analysis.

The analysis shows peaking of the bulk ion in the impurity hole plasma while the impurity profiles becomes hollow and the electron density remains flat throughout the process. The differences in behavior of the plasma species cannot be explained by the radial dependence of the peaking factor found in the dynamic transport analysis. Peaking of the bulk ion was observed in a number of discharges over a broad range of helium puff strength in an ion ITB plasma. What is more in an ion ITB plasma, carbon density profile was found to become more hollow than the helium density profile where the helium density profile was found to be slightly hollow and independent of the helium puff strength. Unfortunately, the study was limited in the weak helium puff regime due to the influx of helium from recycling. The scope of the analysis was also limited in the lower limit of the electron density range. As the electron density is lowered, a higher ion temperature is obtained. However, the lower limit of the electron density is determined by the wall recycling and the exhaust of carbon due to the formation of the impurity hole. Additionally, the ion ITB plasma with the highest ion temperature is only a transient phenomenon. Sustainment of the steady state ion ITB plasma with higher ion and electron temperature by combination of NBI and ECH is planned in the future. A study of the differences between helium and hydrogen peaking factors in an ITB discharge with a very small helium fraction in the plasma core would be interesting for the reactor prospects.

In conclusion, the density peaking of bulk ions due to inward convection (peaking factor $C_{\rm v} > 0$) was observed in the impurity hole plasma with ion internal transport barrier, where the helium and carbon impurity profiles become hollow due to the outward convention ($C_{\rm v} < 0$) in LHD. This is in contrast to the L-mode plasma where the density profile of bulk ions is flat ($C_{\rm v} \sim 0$) and the helium and carbon impurity profiles are flat or peaked depending on the fraction of helium. The results presented in this paper clearly demonstrate co-existence of the inward convection of the hydrogen and the outward convection of carbon at $r_{\rm eff}/a_{99} > 0.5$ due to the momentum exchange between the bulk ion and the impurity ions, which is usually taken into account in the neoclassical transport impurity transport in tokamak [8] but not in helical plasmas [15, 16].

Acknowledgments

The authors would like to thank the technical staff of the Large Helical Device for their support of these experiments. This work is partially supported by a Grant-in-Aid for Scientific Research of Japan Society for the Promotion of Science (JSPS) (No. 15H02336). This work is also partially supported by the National Institute for Fusion Science grant administrative budget (NIFS10ULHH021). This work is also partially supported by the EUROfusion Consortium and has received funding from the Euratom research and training programme 2014-2018 under Grant Agreement No. 633053

References

[1] McCormick K *et al.* 2002 *Phys. Rev. Lett.* **89** 015001
[2] Ida K *et al.* 2003 *Plasma Phys. Control. Fusion* **45** 1931
[3] Burhenn R *et al.* 2003 *Fusion Sci. Technol.* **45** 1931
[4] Braun S *et al.* 2010 *Phys. Plasmas* **17** 072514
[5] Angioni C *et al.* 2011 *Phys. Rev. Lett.* **107** 215003
[6] others C A 2009 *Plasma Phys. Control. Fusion* **51** 124017
[7] Mikkelsen D *et al.* 2014 *Phys. Plasmas* **21** 082302
[8] Wade M *et al.* 2000 *Phys. Rev. Lett.* **84** 282
[9] Ida K *et al.* 2015 *Rev Sci Instrum* **86** 123514
[10] Fonck R *et al.* 1984 *Phys. Rev. Lett.* **52** 530
[11] Wade M *et al.* 1995 *Phys. Plasmas* **2** 2357
[12] Schmitz O *et al.* 2016 *Nucl. Fusion* **56** 106011

[13] Ida K *et al.* 2016 *Plasma Phys. Control. Fusion* **58** 074010
[14] Yoshinuma M *et al.* 2009 *Nucl. Fusion* **49** 062002
[15] Ida K *et al.* 2009 *Phys. Plasmas* **16** 056111
[16] Ido T *et al.* 2010 *Plasma Phys. Control. Fusion* **52** 124025
[17] Ida K *et al.* 2009 *Nucl. Fusion* **49** 095024
[18] Ida K *et al.* 2000 *Rev. Sci. Instrum* **71** 2360
[19] Narihara K *et al.* 2001 *Rev. Sci. Instrum* **72** 1122
[20] Itoh S I 1992 *Phys. Fluids B* **4** 796
[21] Ida K *et al.* 1989 *Nucl. Fusion* **29** 231
[22] Nagaoka K *et al.* 2015 *Nucl. Fusion* **55** 113020
[23] Yokoyama M *et al.* 2008 *Phys. Plasmas* **15** 056111
[24] Nakamura Y *et al.* 2002 *Plasma Phys. Control. Fusion* **44** 2121
[25] Nakamura Y *et al.* 2003 *Nucl. Fusion* **43** 219
[26] Burhenn R *et al.* 2009 *Nucl. Fusion* **49** 065005
[27] Yoshinuma M *et al.* 2015 *Nucl. Fusion* **55** 083017
[28] Goto M *et al.* 2003 *Phys. Plasmas* **10** 1402–1410
[29] Yoshinuma M 2010 Impurity transport of ion itb plasmas on lhd *Proceedings of the 23rd IAEA Fusion Energy Conference* vol 23 (International Atomic Energy Agenc)